

# Shear viscosity from nuclear stopping

Brent Barker

*Department of Biological, Chemical, & Physical Sciences,  
Roosevelt University, Chicago, IL 60605, USA\**

Pawel Danielewicz

*National Superconducting Cyclotron Laboratory and Department of Physics & Astronomy,  
Michigan State University, East Lansing, MI 48824, USA*

(Dated: December 16, 2016)

## Abstract

Within the BUU transport model, we demonstrate correlation between stopping observables and shear viscosity in central nuclear collisions at intermediate energies (on the order of  $10^1$  to  $10^3$  MeV). Consequently, we assess the viscosity of nuclear matter by tuning the in-medium nucleon-nucleon cross section in our transport model to agree with nuclear stopping data. Then we use that cross section to calculate the viscosity self-consistently. We also calculate the ratio of shear viscosity to entropy density to determine how close the system is to the universal quantum lower limit proposed in the context of ultrarelativistic heavy ion collisions.

---

\* bbarker@roosevelt.edu

Knowledge of the shear viscosity is important for understanding the stability of rotating neutron stars, the formation of black holes, and the evolution of supernovae. Besides its immediate practical importance, there have been conjectures regarding a fundamental quantum lower limit on the ratio of shear viscosity to entropy density ( $\eta/s$ ) in a wide range of fluids [1–3]. Among other situations, the limit is thought to be approached in the quark-gluon plasma and accessed in ultrarelativistic heavy ion collisions [4]. The question remains as to whether these quark degrees of freedom are needed to approach such a limit in collisions. We will make a quantitative assessment of how close nuclear matter, as seen in these lower-energy collisions, is to this “perfect liquid” limit.

Many groups have used the characteristics of giant resonances to determine the viscosity of nuclear matter (see references in [5]). Several groups have investigated the  $\eta/s$  ratio for different models utilized in nuclear collisions at intermediate energies, such as statistical multifragmentation [6] and quantum molecular dynamics (QMD) [7]. However, the latter investigations did not link viscosity to specific observables and did not try to establish generality of the results beyond the specifics of the models. Finally, the relaxation-time approach [8] is suitable for order-of-magnitude estimates, but not for quantitative assessments.

In the present work, we use stopping, i.e. the degradation of the projectile longitudinal momentum due to interaction with the target, to constrain the elastic part of the in-medium nucleon-nucleon cross section,  $\sigma_{\text{NN}}^{\text{med}}$ , in a BUU transport model. We do not modify any inelastic NN channels, so the results lose their validity at higher energies when pion production influences the dynamics. Additionally, as our model does not incorporate larger composite fragment production ( $A > 3$ ), some of the stopping observables cannot be extracted at low energies in the same way as for the data. Different strategies for cross section reduction can give the same amount of stopping, so we also test whether viscosity is, in fact, a quantity that matters for stopping, or whether unrelated aspects of the in-medium cross section matter, without a significant correlation of the viscosity with the stopping data. We then use this (model-dependent) cross section to calculate the viscosity of nuclear matter according to this same BUU model, attempting to minimize the model-dependence of the conclusions.

## I. BOLTZMANN-UEHLING-UHLENBECK EQUATION

To describe central nuclear reactions, we use a set of Boltzmann-Uehling-Uhlenbeck (BUU) equations, one for each species  $X$ , describing the time evolution of a Wigner quasi-probability distribution in phase space,  $f_X \equiv f_X(\vec{r}, \vec{p}, t)$ :

$$\frac{\partial f_X}{\partial t} + \frac{\partial \epsilon_{\vec{p}}}{\partial \vec{p}} \frac{\partial f_X}{\partial \vec{r}} - \frac{\partial \epsilon_{\vec{r}}}{\partial \vec{r}} \frac{\partial f_X}{\partial \vec{p}} = I_{X,\text{elastic}} + I_{X,\text{inelastic}}, \quad (1)$$

A prototype equation for the above is the single-particle Liouville equation (or Vlasov equation), with zero on the r.h.s., describing the single-particle evolution of a phase space density in a mean field. In the above,  $\frac{\partial \epsilon_{\vec{p}}}{\partial \vec{p}}$  is the single-particle velocity, and  $\frac{\partial \epsilon_{\vec{r}}}{\partial \vec{r}}$  is the force due to the mean field.

The r.h.s. of Eq. 1 takes into account the effect of elastic and inelastic collisions. The elastic term can be expressed as

$$I_{X,\text{elastic}} = \sum_Y \frac{g_X}{(2\pi\hbar)^3} \int d\vec{p}_Y d\Omega v_{XY} \frac{d\sigma}{d\Omega} \left( \tilde{f}_X \tilde{f}_Y f'_X f'_Y - \tilde{f}'_X \tilde{f}'_Y f_X f_Y \right). \quad (2)$$

The first term accounts for particles with momenta  $\vec{p}'_X$  and  $\vec{p}'_Y$  colliding and acquiring the final momenta  $\vec{p}_X$  and  $\vec{p}_Y$ , thus increasing the occupancy  $f_X$  (gain). The second term describes, correspondingly, a decrease in the occupancy  $f_X$  in a reverse process (loss). Here,  $\tilde{f}_X \equiv 1 - f_X$  represents the Pauli principle blocking scattering into the final state  $\vec{p}_X$ . The rate of scattering is governed by the NN cross section  $\frac{d\sigma}{d\Omega}$  (here, a function of  $\vec{p}_X$ ,  $\vec{p}_Y$ , and  $\Omega$ , the angle between the relative momenta before and after the collision). It is this cross section of which modifications by in-medium effects are explored in Section II.

The second, inelastic term on the r.h.s. of Eq. 1 represents interactions that create or annihilate particles of the given species. Note that in the following sections, only the modification of elastic cross sections by in-medium effects are explored. Therefore, the physical regimes on which conclusions can be drawn are those in which inelastic processes do not significantly affect the dynamics. Once beam energies are high enough, for example, pions are produced early in the collision. This affects the stopping, so until pion cross sections are also addressed, we restrict ourselves to lower energies. Formation and breakup of nuclear clusters is inelastic too, but we restrict it to low densities, so that these processes are significant only after the dynamics significant to stopping have already occurred.

An implementation of a time-dependent solution to the Boltzmann equation set by Danielewicz and collaborators [9–14] is used to describe nuclear collisions. In this implemen-

tation, the Wigner distributions are represented by a large number of test particles. These particles move along classical trajectories under the influence of the mean field and encounter random binary collisions with other test particles that are close to them in position space. With an increase of test particle number, the simulation converges on a better averaged out, stable solution.

### A. Impact parameter selection

Throughout this work, we will be comparing our simulation results to experimental data. In experiment, a range of impact parameters is selected for analysis. It is uncertain what precisely the distribution of those impact parameters is. In the transport simulation, the initial state is prepared with one specific impact parameter. To save computation time, an effective impact parameter,  $b_{\text{eff}}$ , is commonly chosen that represents the median in probability for the impact parameter range. For a range bounded by  $b_{\text{min}}$  and  $b_{\text{max}}$ , the effective impact parameter  $b_{\text{eff}}$  is normally taken from

$$\pi b_{\text{eff}}^2 = \frac{\pi b_{\text{min}}^2 + \pi b_{\text{max}}^2}{2} \tag{3}$$

$$b_{\text{eff}} = \sqrt{\frac{1}{2} (b_{\text{min}}^2 + b_{\text{max}}^2)}$$

In studies of central collisions, often experimental ranges start at  $b_{\text{min}} = 0$ , so  $b_{\text{eff}} = b_{\text{max}}/\sqrt{2}$ . We have tested in several cases that such a single parameter can indeed adequately represent the range, in that results from one parameter agree to a satisfactory degree with those from combining calculations from impact parameters spanning the range.

## II. THE NN CROSS SECTION IN THE NUCLEAR MEDIUM

Looking ahead, comparisons to data make it clear that using the bare nucleon-nucleon cross section in the BUU equation (Eq. 1) overestimates the amount of stopping found in central collisions at intermediate energy. There are several different methods currently used to represent the adjustment to  $\sigma_{\text{NN}}$  in the medium.

Many groups use the assumption that cross sections should scale with the nucleon effective mass [15–17]. This would require the nuclear transition matrix to stay the same

in the medium as in vacuum as in a perturbative situation, so there are questions about its validity. Further, the cross section should also be affected by the isospin asymmetry of the surrounding medium and several other factors, leading Sammaruca to conclude that no simple phenomenological ansatz following effective mass scaling is valid [18].

Some authors simply take  $\sigma_{\text{NN}}^{\text{med}}$  simply as half the free cross section [19, 20], which gives approximately the same cross section reduction as the effective mass scaling. The deficiency of this approximation is that the free NN cross sections are not recovered when the matter becomes dilute.

Following the transition matrix approach, one can derive, in the quasi-particle limit, both the mean field and in-medium cross section, making the development of the BUU equation more self-consistent, in principle, changing both sides of Eq. 1 [21, 22]. With this, the collision modification is only due to the mean field and statistics.

The first phenomenological  $\sigma_{\text{NN}}^{\text{med}}$  in the literature was assumed to change linearly with density [23]. Another phenomenological approach was then taken, where the cross section was assumed to reduce to a geometric unitary limit at high density [13].

In this paper, three scenarios for intermediate cross sections are explored. We resort to those scenarios because the free NN cross sections are found to be too large to describe data. In practical use in the BUU simulation, the  $\sigma_{\text{NN}}^{\text{med}}$  is applied as a reduced probability of each NN collision to occur, compared to  $\sigma_{\text{NN}}^{\text{free}}$ . Thus, each reduced cross section is presented as a reduction factor multiplied by the free cross section. Pauli blocking of the final state is incorporated separately from this reduction factor.

### A. Tempered cross sections

The Tempered cross section reduction scheme [13] is arrived at by considering unitarity. For a particle moving through a medium of number density  $n$ , the scattering partners are distributed at a relative distance of  $\approx n^{-1/3}$ . For two-body collisions to be independent from each other, the cross sections should be no larger than a value of the order of  $n^{-2/3}$ ,

$$\sigma_{\text{NN}}^{\text{med}} \lesssim \sigma_0 \equiv \nu n^{-2/3}, \quad (4)$$

where  $\nu$  is of the order of 1. As the medium becomes more dilute, though, the cross sections should reach their free-space limit. We parameterize the continuous change between the free

and unitary limits with the formula:

$$\sigma_{\text{NN}}^{\text{med}} = \sigma_0 \tanh \left( \frac{\sigma_{\text{NN}}^{\text{free}}}{\sigma_0} \right), \quad (5)$$

where  $\sigma_0$  is defined in Eq. 4 (in principle, other smooth interpolating functions could be used). As energies in an NN subsystem increase, the free NN cross sections become increasingly anisotropic, peaking in the forward and backward directions. Those peaks are tied to higher angular momentum values. When particles are more tightly packed in a medium, these cross sections should be suppressed, relative to cross sections with lower angular momentum. For the anisotropic cross sections, we adopt a modification of Eq. 5:

$$\left( \frac{d\sigma}{d\Omega} \right)^{\text{med}} = \frac{\sigma_0}{4\pi} \tanh \left[ \frac{4\pi}{\sigma_0} \left( \frac{d\sigma}{d\Omega} \right)^{\text{free}} \right] \quad (6)$$

Here, for the purposes of the cross section, particles are treated as distinguishable, even when they belong to the same species. The equation above accomplishes the goal of preferentially suppressing the forward and backward peaks, or high angular-momentum scattering, relative to the more mid angular-momentum scattering. With Eq. 6, the cross sections become low and isotropic in the high-density limit, with the absolute limit on differential cross section of  $\sigma_0/4\pi$ . We stress here again that we treat the particles as distinguishable in the determination of cross section.

## B. Rostock cross sections

Some early microscopic calculations of in-medium cross sections were carried out at the University of Rostock [24], within a thermodynamic T-matrix approach. In their calculation, the cross sections were modified due to Pauli blocking in intermediate states and single-particle energy shifts [25]. Their results were derived assuming that the total momentum of the particles is zero in the frame of the local nuclear matter, to simplify the calculations. We coarsely capture the essence of their results with the following parametrization of the cross section reduction:

$$\sigma_{\text{NN}}^{\text{med}} = \sigma_{\text{NN}}^{\text{free}} \exp \left( -0.6 \frac{\rho/\rho_0}{1 + \left( \frac{T_{\text{c.m.}}}{150 \text{ MeV}} \right)^2} \right), \quad (7)$$

where  $T_{\text{c.m.}}$  is the total kinetic energy of the two interacting particles, in the frame where the local medium is at rest.

### C. Fuchs

Fuchs et al. [26] note that in the BUU equation (Eq. 1), the in-medium mean fields that the particles are subject to on the l.h.s. should be derived consistently with the in-medium NN cross sections  $\sigma$  used in the collision integral in the r.h.s. The basis for these simultaneous alterations in Ref. [26] is the in-medium Dirac-Brueckner T-matrix. Like the Rostock one, this cross section was derived for two particles with total momentum equal to zero in the rest frame of the local medium. This cross section reduction is parameterized here with

$$\sigma_{nn}^{\text{med}} = \sigma_{nn}^{\text{free}} \exp \left( -1.7 \frac{\rho/\rho_0}{1 + \left( \frac{T_{\text{c.m.}}}{12 \text{ MeV}} \right)^{3/2}} \right) \quad (8)$$

$$\sigma_{np}^{\text{med}} = \sigma_{np}^{\text{free}} \exp \left( -1.4 \frac{\rho/\rho_0}{1 + \frac{T_{\text{c.m.}}}{33 \text{ MeV}}} \right). \quad (9)$$

These different cross section reductions will be used to compare predictions from pBUU to stopping data, in order to see which gives the closest match, and thus which one might eventually be used to calculate the viscosity of nuclear matter within a consistent framework.

## III. STOPPING OBSERVABLES

### A. Linear momentum transfer

In a mass-asymmetric collision of a light projectile colliding with a heavy target, one can assess the momentum that is transferred to the target, and thus have a measure of the stopping power — that is, how much the projectile decelerates when it interacts with the target. As in the schematic in Fig. 1, one finds the laboratory-frame velocity of the largest fragment emitted from the collision. Because of the high mass, that fragment is assumed to stem from the target (the “target-like fragment”). The higher its velocity, the more momentum was transferred from the projectile. This corresponds to a higher degree of stopping. To compare the observable across reaction systems, this fragment velocity is divided by that of the center of mass. Since the velocities involved are non-relativistic, they

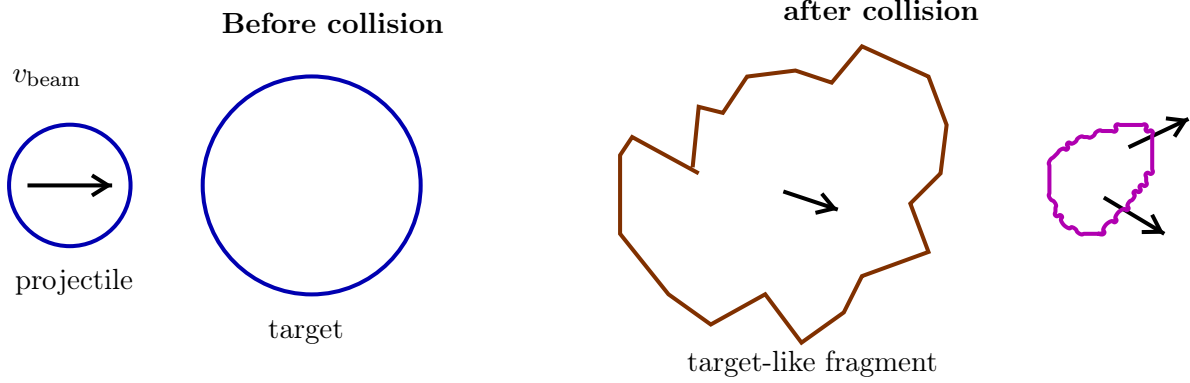


FIG. 1. Schematic of asymmetric collision. Projectile transfers momentum to the target. To assess linear momentum transfer, the longitudinal velocity of the target-like fragment is compared to the velocity of the center-of-mass of the collision.

can be used directly to find the linear momentum transfer (LMT). This observable was originally used to distinguish between direct and compound fission reactions in heavy nuclei [27, 28], then used more generally in nucleus-nucleus collisions [29].

The technique relies on a clear determination of the target-like fragment, and as the beam energy increases, there are more violent collisions and the largest fragment produced becomes lighter. Therefore, the practical energy range for this observable is from around the Coulomb barrier to around 150 MeV/nucleon or so. Additionally, at the high end of this range, intermediate-mass fragments become predominant, which are not present in our model. This is not a difficulty at the energies examined here.

The observable LMT is defined as

$$\text{LMT} = \left\langle \frac{v_{\parallel}}{v_{\text{c.m.}}} \right\rangle, \quad (10)$$

where  $v_{\parallel}$  is the velocity of the target-like residue in the beam direction,  $v_{\text{c.m.}}$  is the velocity of the reaction center of mass. A higher LMT corresponds to a higher degree of stopping.

Experimental [30] and theoretical results for LMT in collisions of a  $^{40}\text{Ar}$  projectile with Cu, Ag, and Au targets are shown in Figs. 2, 3, and 4, respectively. At low energies,  $\text{LMT} \simeq 1$ , indicating formation of a compound system and complete stopping. As beam energy increases, transparency sets in and LMT decreases. In the experiment, it appears that targets were used with natural isotopic content. To determine  $V_{\parallel}$  in the equation



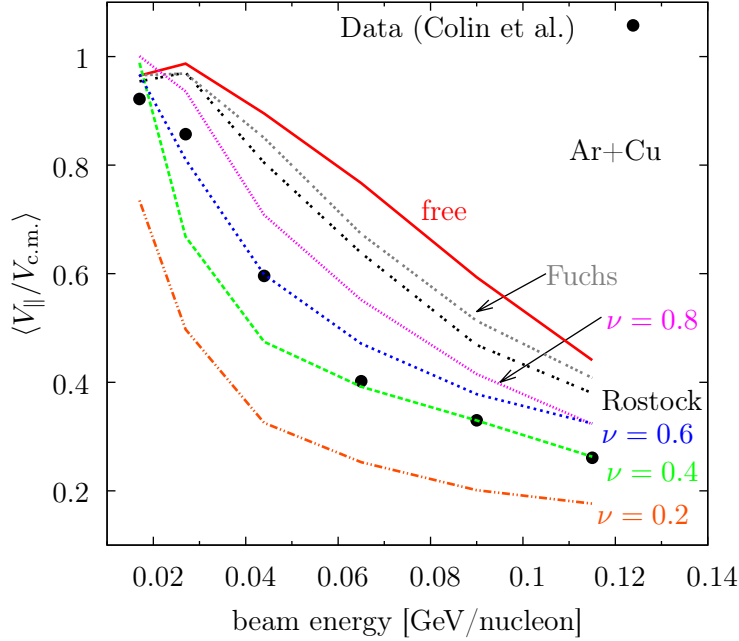


FIG. 2. Linear momentum transfer for  $^{40}\text{Ar} + \text{Cu}$ . Lines represent the theoretical results incorporating different in-medium NN cross sections. The “Tempered” reductions are marked with their tunable parameter  $\nu$ . Symbols represent experimental data [31].

above, a filter on just the heaviest fragments was used, with the assumption that these heaviest fragments provide a good average estimate of the target-like fragment’s longitudinal momentum.

In the BUU calculations, we use  $^{63}\text{Cu}$ ,  $^{107}\text{Ag}$ , and  $^{197}\text{Au}$  for the targets. In central collisions at this energy, the one- or two-neutron differences in the target content should not impact LMT enough to matter. Within our simulation, the target-like fragment is explicitly tracked throughout the collision, and its velocity is directly calculated from the constituent particles. In particular, nucleons that initially belonged to the target and continue to be bound are considered to be part of the TLF. To be considered bound, the particle energy must be at least 6 MeV below the continuum in the local frame. For charged particles, the energy excludes the Coulomb contribution, i.e. the continuum is counted from the top of the local Coulomb barrier.

The various  $\sigma_{\text{NN}}^{\text{med}}$  schemes described in Section II are tested in BUU calculations, with the corresponding results shown with lines in Figs. 2–4 alongside the experimental data.

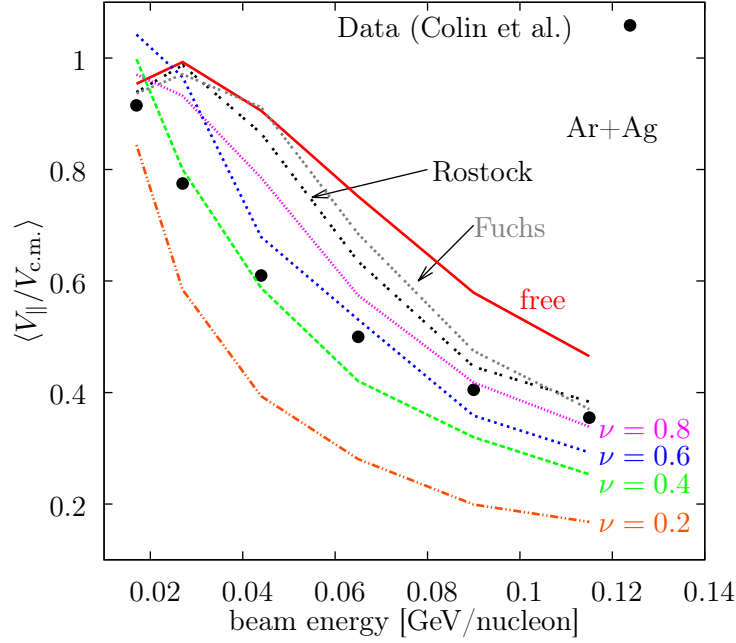


FIG. 3. Linear momentum transfer for  $^{40}\text{Ar} + \text{Ag}$ . Lines represent the theoretical results incorporating different in-medium NN cross sections. The “Tempered” reductions are marked with their tunable parameter  $\nu$ . Symbols represent experimental data [31].

The Rostock and Fuchs reductions, as well as the case with no reduction (“free”), are labeled with their names, while the Tempered CS is marked by its tunable parameter  $\nu$ . It is clear from the LMT figures that the free cross section overestimates the stopping in all three reaction systems, and that the Tempered CS with  $\nu = 0.2$  underestimates it. The Rostock and Fuchs reductions produce LMT values that are very close to each other in all cases, with Fuchs resulting in  $\sim 7\%$  higher values than Rostock in the 65 MeV region.

Focusing on the trends, the free CS results in a linear dependence of LMT on beam energy in all three systems at about 27 MeV and higher, while the reductions all exhibit a positive concavity with energy in the  $^{40}\text{Ar} + \text{Cu}$  and  $^{40}\text{Ar} + \text{Ag}$  cases that more closely resembles the data. In the case of  $^{40}\text{Ar} + \text{Au}$ , all calculated lines show a roughly linear dependence on beam energy, while the experimental data shows an even larger concavity compared to the lighter systems.

Judging by eye, the cross section that best fits the  $^{40}\text{Ar} + \text{Cu}$  and  $^{40}\text{Ar} + \text{Ag}$  data is the Tempered one with  $\nu = 0.4$  or  $0.6$ . In the  $^{40}\text{Ar} + \text{Au}$  reaction, however, due to the

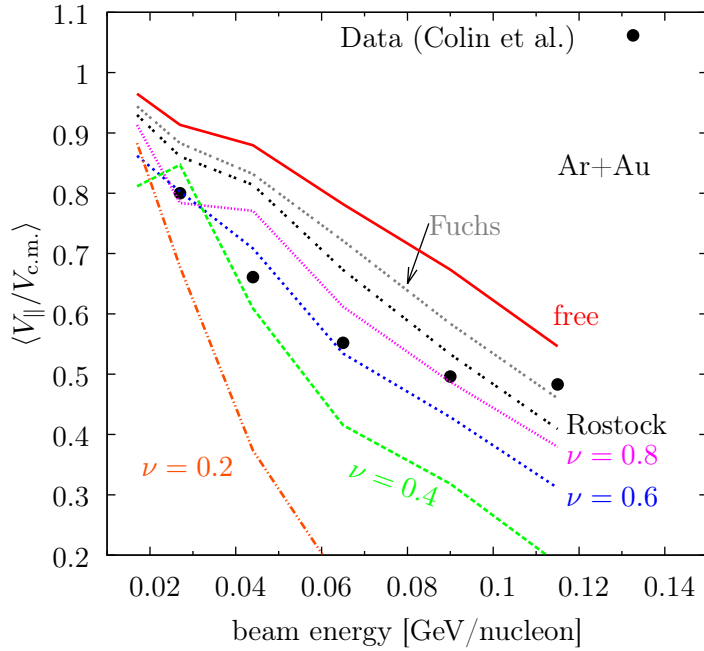


FIG. 4. Linear momentum transfer for  $^{40}\text{Ar}+\text{Au}$ . Lines represent the theoretical results incorporating different in-medium NN cross sections. The “Tempered” reductions are marked with their tunable parameter  $\nu$ . Symbols represent experimental data [31].

combination of effects described in the previous paragraph, the cross section that best fits the data seems to be the Tempered CS with  $\nu = 0.8$ . Note that this determination of  $\sigma_{\text{NN}}^{\text{med}}$  is so-far only valid within the context of this specific model, the Boltzmann transport simulation described in Section I. In Sec. V, we use this cross section to calculate the viscosity of nuclear matter in a self-consistent way, so that the conclusions may become more model-independent.

## B. Rapidity variance ratio

If particles in the hot, dense region of a nuclear collision undergo many collisions (because the radius of the particle-particle cross section becomes comparable to the typical interparticle distance), the region tends to equilibrate, and particles will lose memory of which direction they were originally traveling in. Emission from that region will tend towards isotropy in the reaction center of mass. The more isotropic the emission, the more stopping has generally occurred. The observable  $\text{var}x_z$  provides a measure of this isotropy.

The FOPI Collaboration defines it thusly [32]:

$$varxz = \frac{\Delta y_x}{\Delta y_z}, \quad (11)$$

where  $\Delta y_x$  is the variance of particle rapidity along a direction that is transverse to the beam and fixed in the laboratory frame, which is a random transverse direction in the reaction center-of-mass system.  $\Delta y_z$  is the variance of the particle longitudinal rapidity (along the beam direction). Note that in the calculation, we choose a random transverse direction for each particle, washing out any in-event correlation between these emissions. Thus, we implicitly assume that any correlations in the transverse direction between particle emissions do not affect the  $varxz$  significantly.

Fig. 5 shows the experimental results from FOPI [33] as well as the BUU transport simulation with the various  $\sigma_{NN}^{\text{med}}$  reduction schemes used, for Au + Au, looking at the distribution of protons. The experiment was performed using the heavy ion accelerator SIS at GSI/Darmstadt, and charged particles were detected with a good coverage of angles throughout the  $4\pi$  region, using the FOPI detector and a set of other detectors that provided particle tracking, energy loss determinations, time of flight determination, and charged particle identification. The beam energies spanned the range from 0.09 to 1.5 GeV/nucleon, and the impact parameter selection was limited to  $b_{\text{red}} \equiv b/b_{\text{max}} \lesssim 0.15$ .

Within the variable  $varxz$ , we see that stopping is never complete in central Au + Au reactions, since  $varxz$  tends to stay below 1. Above  $\sim 0.9$  GeV/nucleon, an abrupt decline in stopping takes place. Two factors that begin to matter is that (1) momenta in the center of mass become large compared to the Fermi momentum and that (2) cross sections become anisotropic.

In addition, as beam energy increases, pion production sets in. Eventually, the stopping begins to be dominated by inelastic processes. Since we refrain here from introducing medium-based modifications for inelastic processes, the rise in their importance limits for us the ability to learn from the stopping data. This rise in importance is marked by convergence of predictions for different reductions of elastic cross sections.

Besides looking at convergence of theoretical results as a function of beam energy, we can look directly into the simulations. For example, in the Au + Au collision used in Fig. 5, we can examine the pBUU simulations with the tempered  $\sigma_{NN}^{\text{med}}$ , with  $\nu = 0.6$ , a reasonable parameter. From 90 to 1500 MeV/nucleon, the ratio of peak  $\Delta$  production and absorption rates,

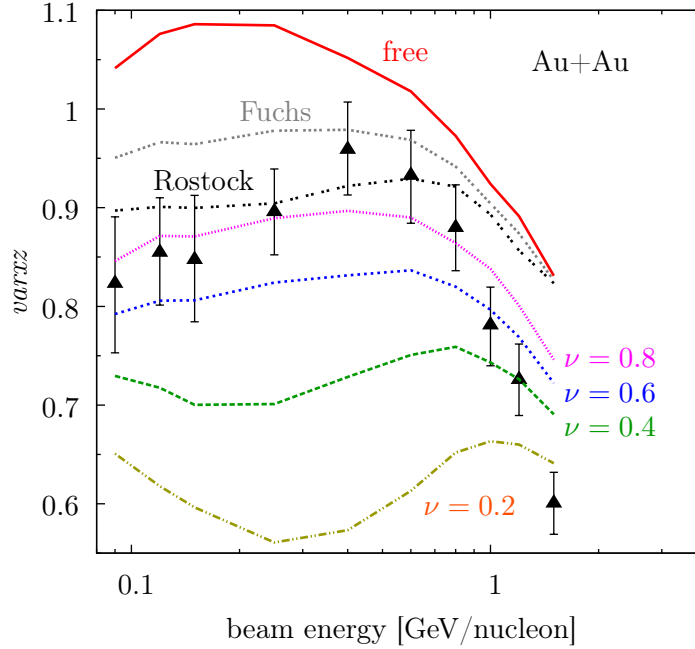


FIG. 5. Stopping observable  $varxz$  for protons in Au + Au collisions at different beam energies at  $b_{\text{red}} < 0.15$ . Lines show the effects of different in-medium reductions of the NN cross section. The “Tempered” reductions are marked with their tunable parameter  $\nu$ . Symbols are experimental data from the FOPI collaboration. [34].

the primary inelastic processes, to peak elastic collision rates varies from 0 to 0.8. Assuming that the inelastic collisions start significantly affecting the reaction dynamics when the ratio is about 0.2 or 0.3, then we should look at beam energies of less than 600 MeV/nucleon. Given that caveat, it seems the  $\sigma_{\text{NN}}^{\text{med}}$  that best fits the data below 600 MeV/nucleon is either  $\nu = 0.8$  or Rostock.

Another caveat regarding our comparison of  $varxz$  calculations to FOPI data concerns production of heavier fragments in collisions. Their number increases as beam energy drops, and they tend to be produced in larger numbers in the colder regions of a reaction (at lower specific entropy), specifically in matter that has avoided the most violent processes in a reaction. This matter will have a greater tendency to maintain the original direction of motion along the beam axis. Unstable fragments can decay into lighter fragments, in particular nucleons, lowering their  $varxz$ , as compared to the situation without secondary decays. Given the lack of fragment production in our calculation, it can be safest to limit

the reliance of the *varxz* conclusions to the energies  $E_{\text{beam}} \lesssim 600 \text{ MeV/nucleon}$  — that is, the peak region in *varxz* in Fig. 5, even when the lower energies support the same conclusions.

In fact, while most of our results are quoted with nucleons, pions, and deltas as the only degrees of freedom in the BUU simulations, there exists an option in the code to activate production and breakup of light  $A \leq 3$  clusters. As a test of robustness of our conclusions, we can activate the cluster production and see whether our conclusions may change. Notably, activating this production does not introduce secondary decays of unstable fragments, but such processes are not likely to be important at more elevated energies, up to  $E_{\text{beam}} \lesssim 600 \text{ MeV/nucleon}$ . Some general concern regarding cluster production when considering stopping is that there may be some double-counting of processes when the production is activated, leading to enhanced stopping. To alleviate this, the production is only allowed at densities  $\rho \lesssim 0.6\rho_0$ , i.e. times and regions with limited impact on momentum transfer between projectile and target systems.

The results with the light cluster production activated are next shown and compared to FOPI data in Fig. 6. We see, indeed, a modest shift in the results for protons. Overall, in Fig. 6, the calculations yield a less pronounced peak in *varxz* as a function of beam energy than data, no matter what suppression in the cross section is used. From the high-energy side, this may be an indication for the suppression of inelastic cross sections in the medium, not just elastic. From the low-energy side, this is likely due to decay of heavier fragments, not present in the calculations. The peak region in *varxz* vs. energy, where the comparison between data and theory may be most telling, seems to be generally best described with the Rostock cross section or the tempered cross section with  $\nu = 0.8$ , regardless of whether the calculation includes cluster production.

Results for *varxz* in Ca+Ca collisions are shown in Fig. 7. Looking at  $E_{\text{beam}} \lesssim 700 \text{ MeV/nucleon}$  and  $b_{\text{red}} < 0.15$  in panel (a), one is left with one experimental point that is straddled by theory results for  $\nu = 0.4$  and  $\nu = 0.6$ , in disagreement with conclusions from Au+Au collisions. However, for a light system such as Ca+Ca, the correlation between observables used to filter the impact parameters and actual impact parameters is much broader in  $b_{\text{red}}$  than for a heavy system such as Au+Au (Even for Au+Au, the uncertainty in the cut-off parameter may be as large as 1–2 fm [35]). If the impact parameter range is assumed to be twice as large in Ca+Ca as nominally following from the fraction of cross section for the filter observables, i.e.  $b_{\text{red}} < 0.30$ , then the results displayed in Fig. 7b

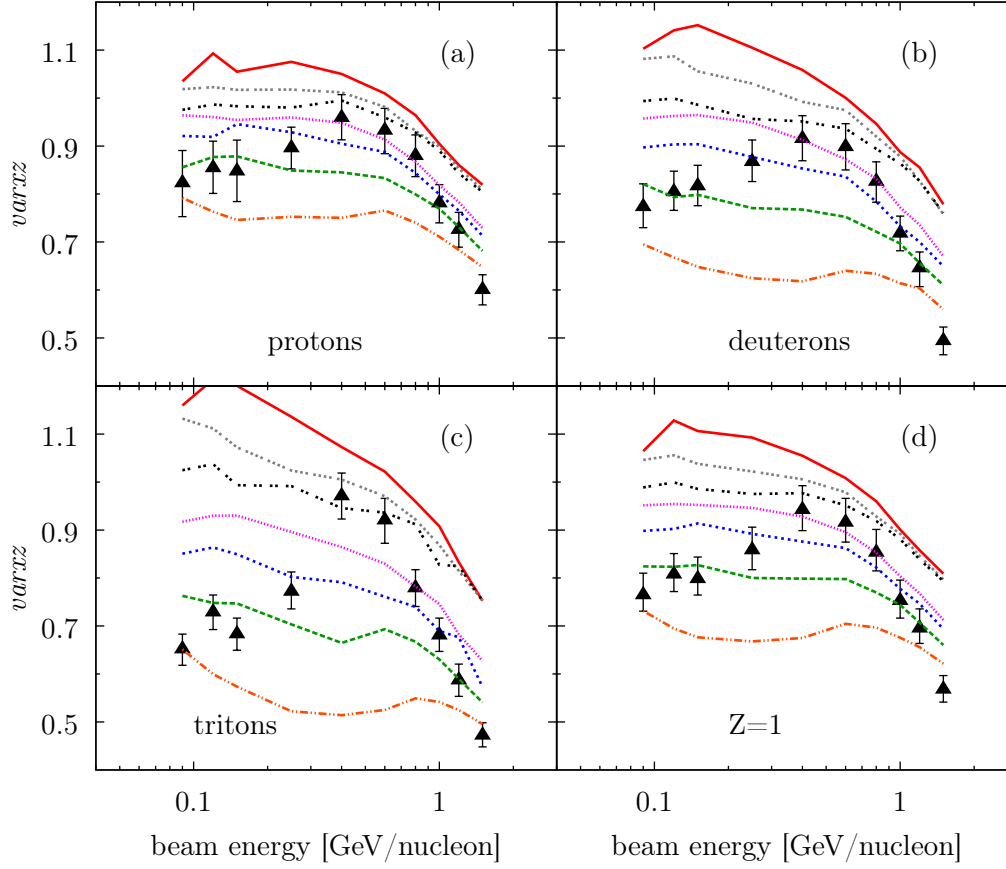
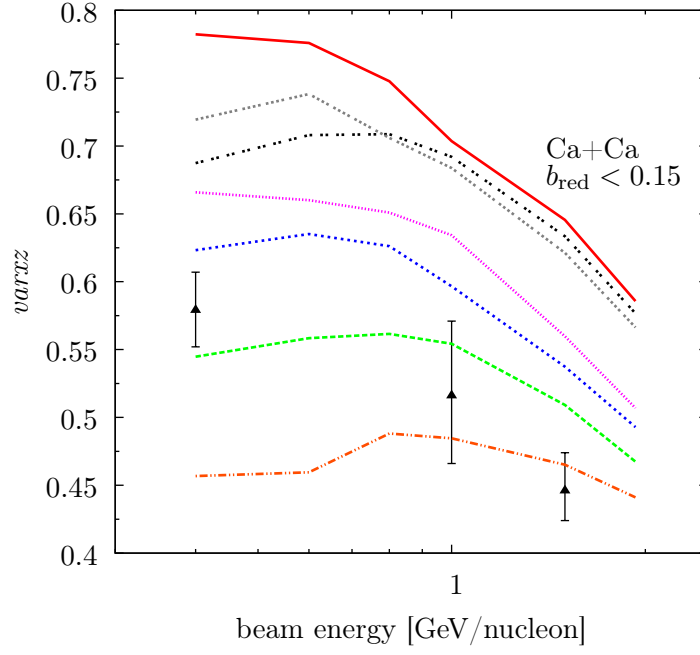


FIG. 6. Analogous to Fig. 5, except that composite particle formation is enabled in the simulations, so a comparison to results for different particle species in the experiment becomes possible.

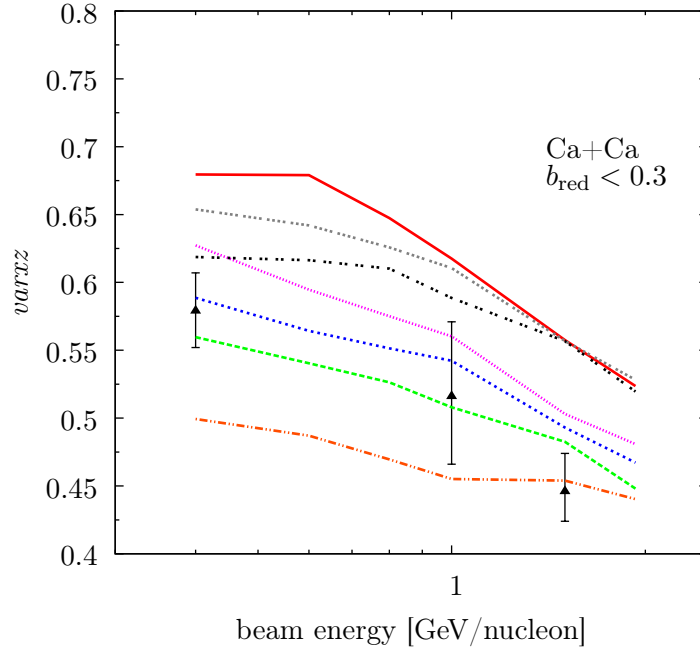
follow and the inferred  $\nu$  in the tempered cross section is now in the range (0.4–0.8), closer to that inferred from Au + Au.

### C. Isospin tracer

Another observable that we use, so-called isospin tracer, attempts to identify the relative yield of particles from the target and projectile in a given region of momentum space by examining isospin content. This is done by studying collisions between mirror nuclei, with identical  $A$  but different  $Z$ , interchanging the projectile and target roles, and comparing the results to those from collisions of identical nuclei.



(a)



(b)

FIG. 7. Stopping observable  $varxz$  for  $^{40}\text{Ca} + ^{40}\text{Ca}$  collisions with centrality selection (a)  $b_{\text{red}} < 0.15$  and (b)  $b_{\text{red}} < 0.30$ . Lines and symbols represent analogous quantities to those in Fig. 5.



The method is described in more detail here:

“The  $(N/Z)$ -tracer method is based on the following idea: let us assume that we are observing the final number of protons,  $Z$  in a given cell of the momentum space. The expected yield  $Z^{\text{Ru}}$  measured for the  $\text{Ru} + \text{Ru}$  reaction is higher than  $Z^{\text{Zr}}$  of the  $\text{Zr} + \text{Zr}$  reaction since Ru has 44 protons as opposed to 40 for Zr. Such measurements using identical projectile and target deliver calibration values  $Z^{\text{Ru}}$  and  $Z^{\text{Zr}}$  for each observed cell. In the case of a mixed reaction,  $\text{Ru} + \text{Zr}$  or  $\text{Zr} + \text{Ru}$ , the measured proton yield  $Z$  takes values intermediate between the calibration values  $(Z^{\text{Ru}}, Z^{\text{Zr}})$ . If, e.g.,  $Z$  is close to  $Z^{\text{Ru}}$  in a  $\text{Ru} + \text{Zr}$  reaction, means that the cell is populated predominantly from nucleons of the Ru projectile while if it is close to  $Z^{\text{Zr}}$  it is mostly populated from nucleons of the Zr target. In this way it is possible to trace back the relative abundance of target to projectile nucleons contributing to a given cell.” [36]

Within the method, one constructs the observable  $R_Z$ , defined as

$$R_Z = \frac{2 \times Z - Z^{\text{Zr}} - Z^{\text{Ru}}}{Z^{\text{Zr}} - Z^{\text{Ru}}}, \quad (12)$$

which assesses relative abundances of the projectile-target nucleons. In this case,  $Z$  represents proton yield, but yield ratios for different particles can also be used [36]. With this definition, one arrives at  $R_Z = 1(-1)$  when a momentum cell gets populated by protons originating exclusively from the Zr (Ru) nucleus. The case of complete stopping would mean that the protons completely mix and for any cell, half come from Zr and half from Ru. Thus, full stopping corresponds to  $R_Z \equiv 0$ .

The experimental results [36], along with results from the BUU transport model, with the  $Z$  in  $R_Z$  representing proton yield, for collisions between  $^{96}\text{Zr}$  and one of its mirror nuclei,  $^{96}\text{Ru}$ , are shown in Fig. 8, for beam energy of 400 MeV/nucleon and  $b_{\text{red}} < 0.12$ .

As rapidity (in the center of mass) gets more negative, the momentum cells are increasingly populated by protons from the target, according to  $R_Z$ . This makes sense, as the target’s particles are more likely to persist in the backward rapidity region. As the bins closer to midrapidity are examined, it is seen that those bins get populated by protons from both colliding nuclei, as  $R_Z$  is close to zero there.

It is clear from Fig. 8 that use of the free NN cross section overestimates the stopping or mixing in this case, as described by the  $R_Z$  observable. It seems that the  $\sigma_{\text{NN}}^{\text{med}}$  best fitting

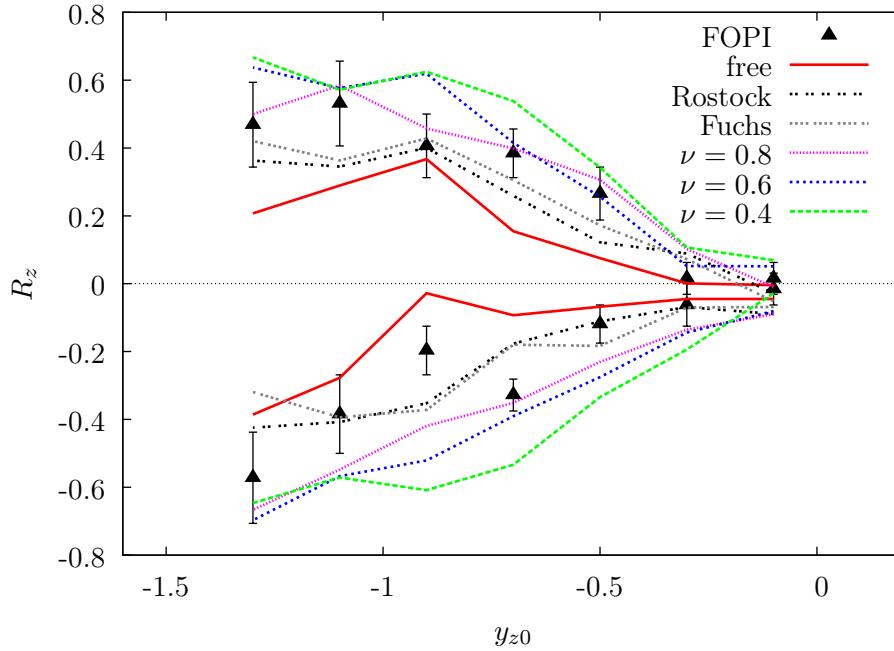


FIG. 8. Isospin tracer observable for central collisions of  $^{96}\text{Zr} + ^{96}\text{Ru}$  (bottom) and  $^{96}\text{Ru} + ^{96}\text{Zr}$  (top) at 400 MeV/nucleon vs. scaled center-of-mass rapidity, where  $y_0 = -1$  is the initial projectile rapidity. Data is from the FOPI collaboration [36]. A tendency of  $R_z$  to stay closer to zero at finite rapidities indicates a higher degree of mixing, and thus stopping.

the data here is either Rostock, Fuchs, or Tempered with  $\nu \sim 0.8$ . The  $R_z$  observable is challenging for Monte Carlo calculations, due to statistical fluctuations that get emphasized in the subtraction of similar values,  $Z^{\text{Zr}} - Z^{\text{Ru}}$ , and further amplified in the division by the resulting small number.

#### D. Sensitivity to Equation of State

The equation of state (EOS) of nuclear matter describes how the energy and pressure change with density and temperature. It is a prime bulk characteristic of nuclear systems reflecting the operating nuclear forces [37]. The FOPI Collaboration found some dependence of the stopping on the EOS [33], specifically on the compressibility of nuclear matter, within the Isospin Quantum Molecular Dynamics (IQMD) model [38]. Here, we test whether we can observe any such sensitivity. An excessive sensitivity of observables to the EOS could hamper the efforts to learn about the cross sections in a manner independent of it.

observable	reaction system	energies [MeV]	best cross section reduction
LMT	$^{40}\text{Ar} + \text{Cu}$	17–115	Tempered w/ $0.4 \leq \nu \leq 0.6$
LMT	$^{40}\text{Ar} + \text{Ag}$	17–115	Tempered w/ $0.4 \leq \nu \leq 0.6$
LMT	$^{40}\text{Ar} + \text{Au}$	27–115	Tempered w/ $\nu = 0.8$
<i>varxz</i>	$\text{Au} + \text{Au}$	90–1500	Tempered w/ $\nu = 0.8$ or Rostock
<i>varxz</i>	$\text{Ca} + \text{Ca}$	400–1500	Tempered w/ $0.4 \leq \nu \leq 0.8$
$R_z$	$^{96}\text{Zr} + ^{96}\text{Ru}$ (and inverse)	400	Tempered w/ $\nu = 0.8$ , Rostock, or Fuchs

TABLE I. Summary of cross section determination results. No single cross section reduction is favored universally, though Tempered with  $\nu = 0.6$  or  $0.8$  appears to be the best compromise.

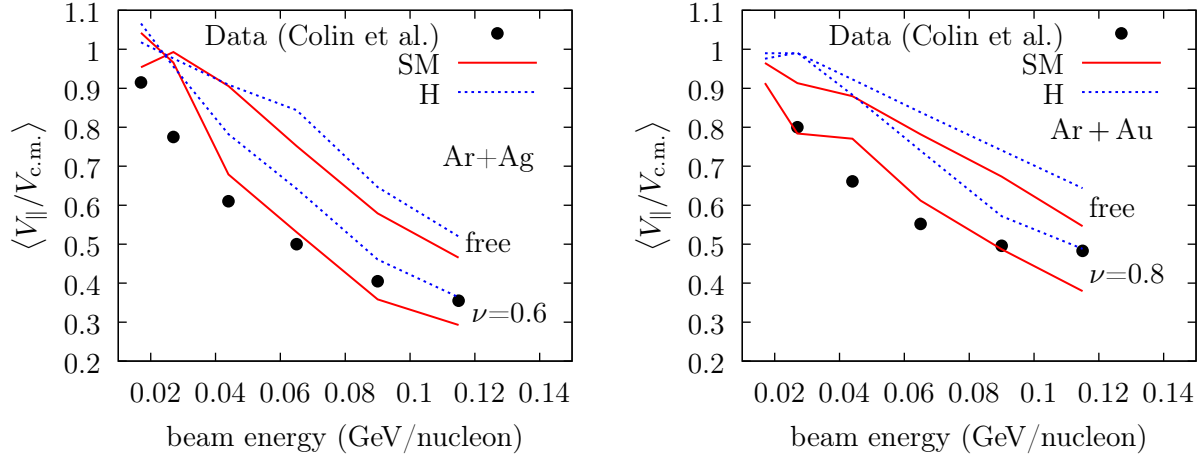
To remind, the compressibility of nuclear matter,  $K$ , is a key input to calculations of neutron stars and some supernovae. It is conventionally defined [39] as

$$K = 9\rho_0 \left. \frac{\partial^2(E/A)}{\partial \rho^2} \right|_{\rho=\rho_0}. \quad (13)$$

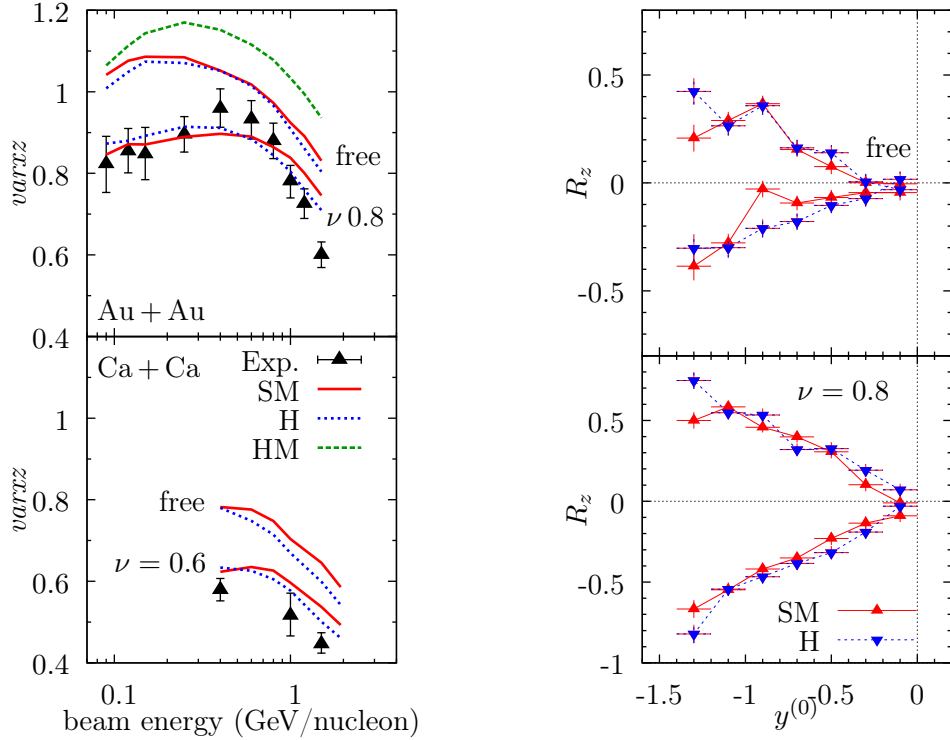
In Fig. 9, effects of two choices of compressibility, as well as of momentum-dependence, are shown. ‘S’ refers to a soft compressibility,  $K = 210$  MeV, while ‘H’ refers to a stiff or “hard” compressibility,  $K = 380$  MeV. ‘M’ refers to the inclusion of momentum-dependence in the mean field, yielding nucleon effective mass at normal density and Fermi momentum of  $m^*/m = 0.7$ . Neither the high incompressibility nor lack of momentum dependence are realistic, but are incorporated here to illustrate any characteristic changes in results.

It can be seen in Fig. 9 that both increase in incompressibility and inclusion of momentum dependence can increase stopping, just as a higher cross section. Even though, physically, the momentum dependence is necessary, and the incompressibility is known to be moderate, it is apparent from Fig. 9 that the conclusions drawn from *varxz* and  $R_Z$  can be less robust than those drawn from LMT. This is because the most uncertain quantity currently pertaining to EOS is incompressibility. In Fig. 9, it may be seen that a switch from moderate to high incompressibility can have as much impact on *varxz* or  $R_Z$  as inclusion of momentum dependence in the mean field. However, the impact of the switch on LMT is more muted.

A summary of the stopping observables that were investigated and the optimal  $\sigma_{\text{NN}}^{\text{med}}$  for each is given in Table I.



(a) linear momentum transfer



(a)  $varxz$

(b) isospin tracer

FIG. 9. EOS dependence of stopping observables. S (H) refers to a soft (stiff) compressibility, while M refers to the inclusion of momentum-dependence in the mean field. SM and H are limiting combinations, and they give similar predictions for stopping observables  $varxz$  and isospin tracer  $R_z$ . However, LMT is as sensitive to these settings as it is to cross section reductions, so that observable is somewhat less robust as far as deciding on the best cross section reduction is concerned.

#### IV. CROSS SECTION REDUCTION AND PHYSICS CONCLUSIONS

In-medium cross sections are obviously not directly observable, and they are tied to the transport equation that relies on the concept of quasiparticles, which brings in a level of phenomenology. So a question might be asked whether more robust conclusions may be drawn from studies of stopping that extend beyond the cross sections. To illustrate the precarious nature of the conclusions on cross sections, we show in Fig. 10a the collision number in Au + Au collisions at 400 MeV/nucleon obtained in simulations, with three different in-medium cross sections: free-space, Rostock, and tempered with  $\nu = 0.8$ . The stopping is similar in those collisions for the Rostock and  $\nu = 0.8$  cross sections when quantified in terms of  $varxz$  and significantly reduced compared to free cross sections, as seen in Fig. 5. Yet, in spite of the similar stopping in that figure, the collision count for the two cross sections is different by a factor of 2 in Fig. 10a. Apparently, the stopping does not directly correlate to the typical elementary cross section in a reaction, which in turn does not bode well for reaching physics conclusions from stopping.

Taking another perspective, the collision count includes some collisions that are hard, occurring at high relative velocity with large momentum transfer, and some that are soft, occurring at low relative velocity and low momentum transfer. Those soft collisions contribute little to momentum transfer across the system as represented by observables such as LMT,  $varxz$ , or  $R_Z$ . Instead, one can consider that the most elementary macroscopic characteristics for a system, which are tied to cross sections, are transport coefficients. The one tied directly to momentum transfer is the shear viscosity, and it involves so-called transport cross sections — the differential cross sections scaled with weights that increase with relative momentum and scattering angle.

In the shear viscosity coefficient  $\eta$ , derived for the BUU equation in Ref [40] (see also [41]),

$$\eta = \frac{5T}{9} \frac{(\int d\vec{p}_1 f_1 p_1^2)^2}{\int d\vec{p}_1 d\vec{p}_2 d\Omega f_1 f_2 \tilde{f}'_1 \tilde{f}'_2 v_{12} \frac{d\sigma}{d\Omega} q_{12}^4 \sin^2 \theta}, \quad (14)$$

the elastic scattering cross section is scaled with a factor  $q^4 \sin^2 \theta$ , which emphasizes large relative momenta  $q$ , where  $q_{12} = |\vec{p}_1 - \vec{p}_2|/2$ , and wide scattering angles  $\theta$ . We next show in Fig.10b the collision count now with the collisions weighted with this  $q^4 \sin^2 \theta$  factor. The weighted collision count is similar for the Rostock and  $\nu = 0.8$  cross sections, consistent

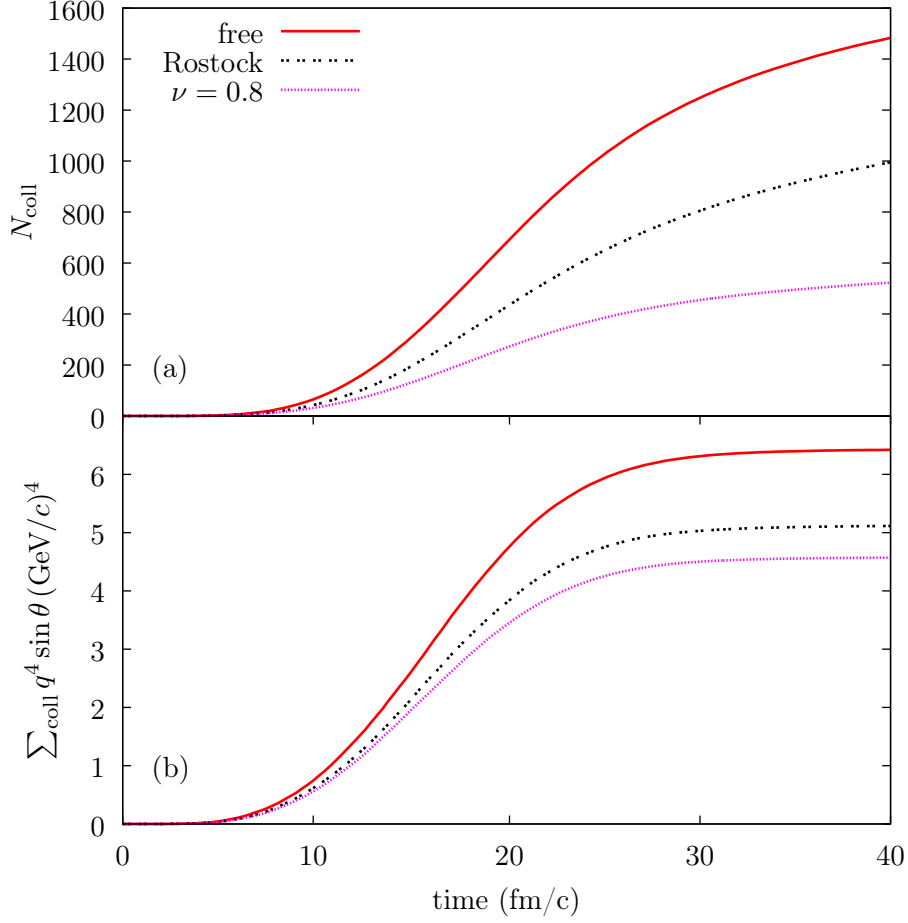


FIG. 10. Number of elastic NN collisions vs. time in central Au + Au collisions at 400 MeV/nucleon, for three different in-medium cross sections. Panels (a) and (b) show, respectively, net number of collisions and number of collisions weighted with the viscous weight.

with  $varxz$  values being similar for those two cross sections in Fig. 5. To provide more insight, in Fig. 10 we plot the unweighted (top) and weighted (bottom) collision counts at 100 fm/c vs.  $varxz$ , for a variety of  $\sigma_{NN}^{med}$ . While the stopping correlates with the unweighted collision count, the correlation is fairly broad, with the count differing even by a factor of 2 for different plausible cross section reduction. Here, again, one can see that the stopping poorly tests the typical elementary cross section in collisions. However, the correlation of the stopping is fairly tight with the collision count when the collisions are weighted with the viscous weight. The broader systematics further support the view that the stopping tests transport cross sections and more broadly the medium shear viscosity.

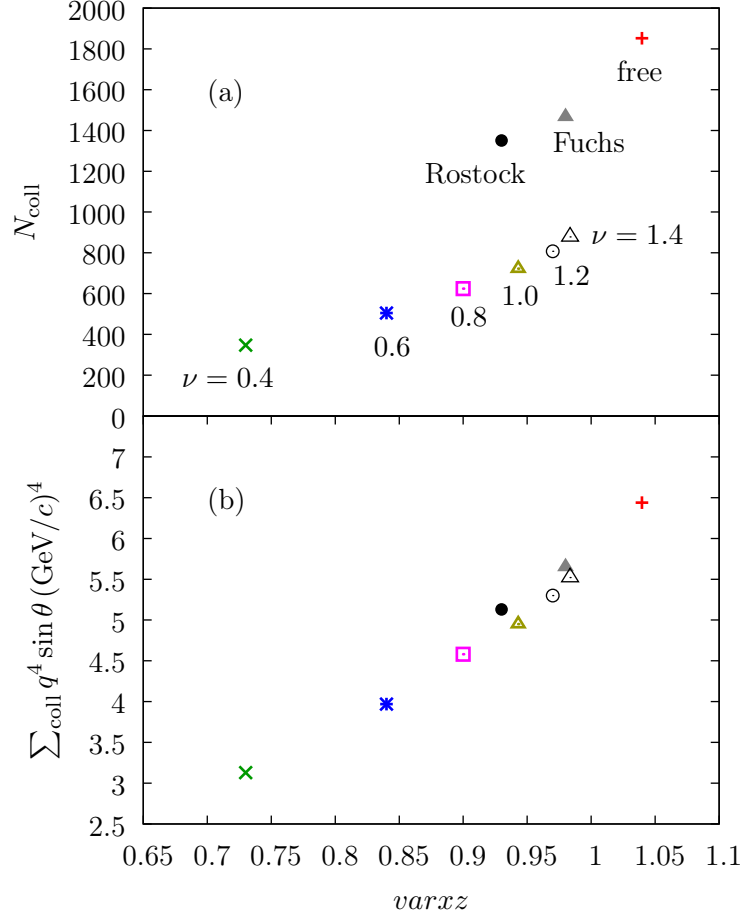


FIG. 11. Relation between the number of nucleon-nucleon collisions that took place up until 100 fm/c and the stopping observable  $varxz$  for the central 400 MeV/nucleon collision. The top panel shows the unweighted collision number, and the bottom panel shows the number weighted with the viscous weight. The weighted collision number rises monotonically with the stopping, unlike the unweighted number.

## V. SHEAR VISCOSITY

As a toy model to introduce the concept of viscosity, we describe laminar shear in a classical system. Consider two plates, with fluid between them, moving in antiparallel directions, in the steady state. The layer adjacent to one plate induces a shear stress,  $\tau$ , on the layer of fluid below it, causing that layer to have a velocity  $v(y - dy) < v(y)$ . That layer induces a shear stress on the layer under it, and so on. In the linear response approximation, these velocities can be related using the equation  $\tau = \eta(\partial v / \partial y)$ , where  $\hat{y}$  is perpendicular to

the plates. Here,  $\eta$  is the coefficient of shear viscosity, which is a measure of the efficiency of the momentum transfer in the fluid.

### A. Viscosity from BUU

As Eq. 14 is derived using the same assumptions as the transport model used to constrain the  $\sigma_{\text{NN}}^{\text{med}}$ , that cross section can be inserted into this equation to find a viscosity coefficient  $\eta$  that is hopefully of greater generality than the transport model itself. The calculation is performed with the effective mass described in Section IIID, which tends to increase the viscosity somewhat.

The results of such calculations are displayed in Fig. 12. At all densities and cross section reductions presented, the viscosity grows indiscriminately at low temperatures. This occurs when the nucleon system becomes degenerate and collisions become strongly Pauli-suppressed with the weighted rate in the denominator in Eq. 14 tending towards zero. As temperatures increase and Pauli effects diminish, the collisions become more frequent. The viscosity goes through a minimum and at high temperatures, it behaves in a classical fashion, growing like  $\sqrt{T}$ . Eventually, inelastic processes set in and calculation of viscosity using just elastic processes in Eq. 14 will start overestimating the viscosity. For situations where consideration of only elastic cross sections is still justified, we demonstrated that the stopping data imply a significant in-medium cross section reduction, as compared to free, and thus an enhancement of the shear viscosity as compared to that calculated with free cross sections. For reference, shear viscosity calculated with free cross sections and velocities is also given in Fig. 12.

We now use our newly determined viscosity to explore how close nuclear matter is to being a “perfect fluid”.

### B. Lower quantum limit of ratio of viscosity to entropy density

It has been found theoretically that certain strong coupling limits of gauge theories have a constant ratio of shear viscosity to entropy density regardless of the metric used [1, 2],

$$\frac{\eta}{s} = \frac{1}{4\pi}. \quad (15)$$



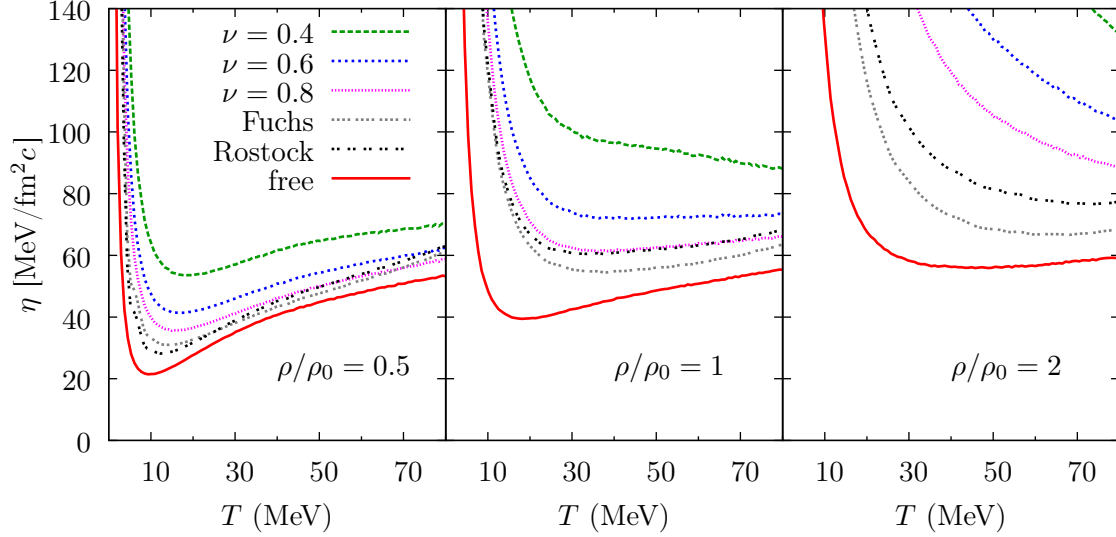


FIG. 12. Shear viscosity for different temperatures, densities, and in-medium cross sections in the Boltzmann equation.

Moreover, it has been speculated that this value represents a lower limit for all relativistic, finite temperature quantum field theories with zero chemical potential, and for single-component nonrelativistic gases of particles with spin 0 or 1/2 [2]. We calculate this ratio at intermediate energies to find the proximity of nuclear matter at this energy to this conjectured lower limit.

To find the ratio  $\eta/s$ , we calculate  $\eta$  and  $s$  separately. To find the entropy density, we utilize the model's ability to describe deuteron yields and use equilibrium conditions relating the ratio of the yield of deuterons and deuteron-like correlations to that of total charge, following the prescriptions of Bertsch and Cugnon [42] as formulated in Ref. [43]. We reproduce the formula here:

$$\sigma = S/A = 3.945 - \ln(N_{\text{d-like}}/Z) - \frac{1}{8}N_{\text{d-like}}/Z, \quad (16)$$

where  $N_{\text{d-like}} = N_{\text{d}} + \frac{3}{2}(N_{\text{t}} + N_{\text{h}}) + 3N_{\alpha} + \dots$  and  $Z = N_{\text{p}} + N_{\text{d}} + N_{\text{t}} + 2(N_{\text{h}} + N_{\alpha}) + \dots$  [44]. The bulk of the entropy is produced in regions of hot, dense matter, during the compression and thermalization phase of the reaction. This is also where the stopping signals are generated. Therefore the density and temperature in that space-time region should be used to determine the entropy per volume,  $s = \sigma n$ , as well as the temperature at which to find the viscosity. In the simulation, we choose a 2 fm-radius spherical region centered at the reaction center of

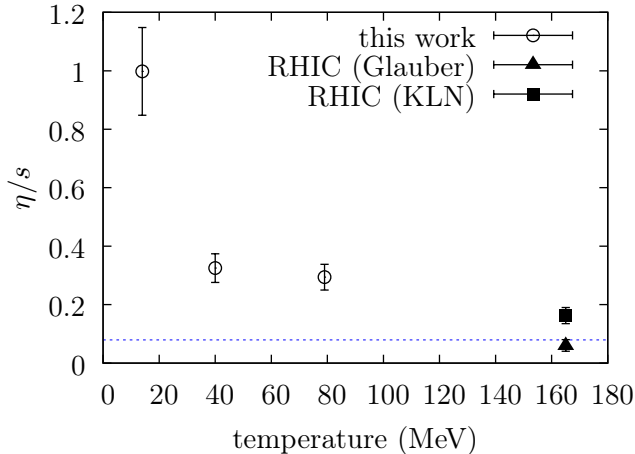


FIG. 13. This work's estimate for  $\eta/s$  values in selected reactions (open circles), alongside the estimates arrived at RHIC energies using the KLN model (square) and the Glauber model (triangle). The conjectured lower quantum limit,  $1/4\pi$ , is shown in a dotted line.

mass, during the time of maximal density in that region. The temperature is found assuming the momentum distribution of the nucleons approximates that of a degenerate relativistic Fermi gas.

We choose several representative reactions to find the characteristic temperatures and densities reached at intermediate energies. Listed here in order of decreasing  $\eta/s$  and increasing maximal temperature, as represented by open circles in Fig. 13, they are  $^{197}\text{Au} + ^{197}\text{Au}$  at beam energies of 100, 400, and 1000 MeV/nucleon, each with a reduced impact parameter  $b_{\text{red}} = 1.5$ . The trend of the nuclear matter looks to match recent findings at RHIC energies, using the Glauber [45] and KLN [46] models in a Monte Carlo Bayesian framework [47], though here at a much lower beam energy. Indeed, as the temperature approaches the critical temperature for nuclear matter,  $\sim 170$  MeV [48],  $\eta/s$  is seen to approach the conjectured lower bound.

## VI. CONCLUSION

We investigated the viscosity of nuclear matter by adjusting the in-medium nucleon-nucleon cross section to fit nuclear stopping data with several different stopping observables across a wide range of nuclear mass and beam energy. We found that, for pBUU, an in-medium reduction in the NN cross section is necessary to match a variety of experimental

data, and that this reduction is stable with respect to different realistic choices of the nuclear equation of state. We used the modified 2-body collision count to argue that our stopping observables are tied to the viscosity. We then calculated the shear viscosity and found that it is enhanced due to the medium effects, with relative enhancement growing with density. We also calculated the ratio of shear viscosity to entropy density,  $\eta/s$ , to determine the proximity of our reaction systems to the conjectured lower quantum limit. We found that the ratio follows a trend that matches with ultrarelativistic heavy ion collisions.

## ACKNOWLEDGMENTS

This work was supported by the US National Science Foundation under Grants PHY-1068571 and PHY-1403906.

- 
- [1] P. Danielewicz and M. Gyulassy, Physical Review D **31**, 53 (1985).
  - [2] P. K. Kovtun, D. T. Son, and A. O. Starinets, Phys. Rev. Lett. **94**, 111601 (2005).
  - [3] T. Schäfer, Annual Review of Nuclear and Particle Science **64**, 125 (2014).
  - [4] R. A. Lacey, N. N. Ajitanand, J. M. Alexander, P. Chung, W. G. Holzmann, M. Issah, A. Taranenkov, P. Danielewicz, and H. Stöcker, Phys. Rev. Lett. **98**, 092301 (2007).
  - [5] N. Auerbach and S. Shlomo, Physical Review Letters **103**, 172501 (2009).
  - [6] S. Pal, Phys. Rev. C **81**, 051601 (2010).
  - [7] C. Zhou, Y. Ma, and D. Fang, Plasma Science and Technology **14**, 585 (2012).
  - [8] J. Xu, L.-W. Chen, C. M. Ko, B.-A. Li, and Y.-G. Ma, *Shear viscosity of neutron-rich nucleonic matter near its liquid-gas phase transition*, arXiv e-print 1306.5361 (2013).
  - [9] P. Danielewicz and G. Bertsch, Nuclear Physics A **533**, 712 (1991).
  - [10] P. Danielewicz and Q. Pan, Phys. Rev. C **46**, 2002 (1992).
  - [11] Q. Pan and P. Danielewicz, Phys. Rev. Lett. **70**, 2062 (1993).
  - [12] P. Danielewicz, Nuclear Physics A **673**, 375 (2000).
  - [13] P. Danielewicz, Acta Phys. Pol. B **33**, 45 (2002), acta Phys.Polon. B33 (2002) 45-64.
  - [14] B. Barker, *Dissipation and dynamics in quantum many-body systems*, Ph.D., Michigan State University, East Lansing, MI, USA (2014).

- [15] V. R. Pandharipande and S. C. Pieper, Phys. Rev. C **45**, 791 (1992).
- [16] D. Persram and C. Gale, Phys. Rev. C **65**, 064611 (2002).
- [17] B.-A. Li and L.-W. Chen, Phys. Rev. C **72**, 064611 (2005).
- [18] F. Sammarruca, Eur. Phys. J. A **50**, 22 (2014).
- [19] C. Yanhuang and M. Di Toro, Phys. Rev. C **39**, 105 (1989).
- [20] T. Gaitanos, M. Colonna, M. Di Toro, and H. Wolter, Physics Letters B **595**, 209 (2004).
- [21] T. Alm, G. Röpke, and M. Schmidt, Phys. Rev. C **50**, 31 (1994).
- [22] T. Gaitanos, C. Fuchs, and H. Wolter, Physics Letters B **609**, 241 (2005).
- [23] G. D. Westfall, W. Bauer, D. Craig, M. Cronqvist, E. Gaultieri, S. Hannuschke, D. Klakow, T. Li, T. Reposeur, A. M. Vander Molen, W. K. Wilson, J. S. Winfield, J. Yee, S. J. Yennello, R. Lacey, A. Elmaani, J. Lauret, A. Nadasen, and E. Norbeck, Phys. Rev. Lett. **71**, 1986 (1993).
- [24] T. Alm, G. Röpke, and M. Schmidt, Physical Review C **50**, 31 (1994).
- [25] T. Alm, G. Röpke, W. Bauer, F. Daffin, and M. Schmidt, Nuclear Physics A **587**, 815 (1995).
- [26] C. Fuchs, A. Faessler, and M. El-Shabshiry, Phys. Rev. C **64**, 024003 (2001).
- [27] W. J. Nicholson and I. Halpern, Phys. Rev. **116**, 175 (1959).
- [28] T. Sikkeland, E. L. Haines, and V. E. Viola, Phys. Rev. **125**, 1350 (1962).
- [29] V. E. Viola, B. B. Back, K. L. Wolf, T. C. Awes, C. K. Gelbke, and H. Breuer, Phys. Rev. C **26**, 178 (1982).
- [30] E. Colin, R. Sun, N. N. Ajitanand, J. M. Alexander, M. A. Barton, P. A. DeYoung, A. Elmaani, C. J. Gelderloos, E. E. Gaultieri, D. Guinet, S. Hannuschke, J. A. Jasma, L. Kowalski, R. A. Lacey, J. Lauret, E. Norbeck, R. Pak, G. F. Peaslee, M. Stern, N. T. B. Stone, S. D. Sundbeck, A. M. Vander Molen, G. D. Westfall, and J. Yee, Phys. Rev. C **57**, R1032 (1998).
- [31] E. Colin, R. Sun, N. N. Ajitanand, J. M. Alexander, M. A. Barton, P. A. DeYoung, A. Elmaani, C. J. Gelderloos, E. E. Gaultieri, D. Guinet, S. Hannuschke, J. A. Jasma, L. Kowalski, R. A. Lacey, J. Lauret, E. Norbeck, R. Pak, G. F. Peaslee, M. Stern, N. T. B. Stone, S. D. Sundbeck, A. M. Vander Molen, G. D. Westfall, and J. Yee, Physical Review C **57**, R1032 (1998).
- [32] W. Reisdorf, M. Stockmeier, A. Andronic, M. Benabderrahmane, O. Hartmann, N. Herrmann, K. Hildenbrand, Y. Kim, M. Kiš, P. Koczoń, T. Kress, Y. Leifels, X. Lopez, M. Merschmeyer, A. Schüttauf, V. Barret, Z. Basrak, N. Bastid, R. Čaplar, P. Crochet, P. Dupieux, M. Dželalija, Z. Fodor, Y. Grishkin, B. Hong, T. Kang, J. Kecskemeti, M. Kirejczyk, M. Korolija,

- R. Kotte, A. Lebedev, T. Matulewicz, W. Neubert, M. Petrovici, F. Rami, M. Ryu, Z. Seres, B. Sikora, K. Sim, V. Simion, K. Siwek-Wilczyńska, V. Smolyankin, G. Stoicea, Z. Tyimiński, K. Wiśniewski, D. Wohlfarth, Z. Xiao, H. Xu, I. Yushmanov, and A. Zhilin, *Nuclear Physics A* **781**, 459 (2007).
- [33] W. Reisdorf, A. Andronic, R. Auerbeck, M. Benabderrahmane, O. Hartmann, N. Herrmann, K. Hildenbrand, T. Kang, Y. Kim, M. Kiš, P. Koczoń, T. Kress, Y. Leifels, M. Merschmeyer, K. Piasecki, A. Schüttauf, M. Stockmeier, V. Barret, Z. Basrak, N. Bastid, R. Čaplar, P. Crochet, P. Dupieux, M. Dželalija, Z. Fodor, P. Gasik, Y. Grishkin, B. Hong, J. Kecskemeti, M. Kirejczyk, M. Korolija, R. Kotte, A. Lebedev, X. Lopez, T. Matulewicz, W. Neubert, M. Petrovici, F. Rami, M. Ryu, Z. Seres, B. Sikora, K. Sim, V. Simion, K. Siwek-Wilczyńska, V. Smolyankin, G. Stoicea, Z. Tyimiński, K. Wiśniewski, D. Wohlfarth, Z. Xiao, H. Xu, I. Yushmanov, and A. Zhilin, *Nuclear Physics A* **848**, 366 (2010).
- [34] W. Reisdorf, A. Andronic, R. Auerbeck, M. Benabderrahmane, O. Hartmann, N. Herrmann, K. Hildenbrand, T. Kang, Y. Kim, M. Kiš, P. Koczoń, T. Kress, Y. Leifels, M. Merschmeyer, K. Piasecki, A. Schüttauf, M. Stockmeier, V. Barret, Z. Basrak, N. Bastid, R. Čaplar, P. Crochet, P. Dupieux, M. Dželalija, Z. Fodor, P. Gasik, Y. Grishkin, B. Hong, J. Kecskemeti, M. Kirejczyk, M. Korolija, R. Kotte, A. Lebedev, X. Lopez, T. Matulewicz, W. Neubert, M. Petrovici, F. Rami, M. Ryu, Z. Seres, B. Sikora, K. Sim, V. Simion, K. Siwek-Wilczyńska, V. Smolyankin, G. Stoicea, Z. Tyimiński, K. Wiśniewski, D. Wohlfarth, Z. Xiao, H. Xu, I. Yushmanov, and A. Zhilin, *Nuclear Physics A* **848**, 366 (2010).
- [35] A. Andronic, J. Łukasik, W. Reisdorf, and W. Trautmann, in *Dynamics and Thermodynamics with Nuclear Degrees of Freedom*, edited by P. Chomaz, F. Gulminelli, W. Trautmann, and S. J. Yennello (Springer Berlin Heidelberg, 2006) pp. 31–46.
- [36] F. Rami, Y. Leifels, B. de Schauenburg, A. Gobbi, B. Hong, J. P. Alard, A. Andronic, R. Auerbeck, V. Barret, Z. Basrak, N. Bastid, I. Belyaev, A. Bendarag, G. Berek, R. Čaplar, N. Cindro, P. Crochet, A. Devismes, P. Dupieux, M. Dželalija, M. Eskef, C. Finck, Z. Fodor, H. Folger, L. Frayse, A. Genoux-Lubain, Y. Grigorian, Y. Grishkin, N. Herrmann, K. D. Hildenbrand, J. Kecskemeti, Y. J. Kim, P. Koczon, M. Kirejczyk, M. Korolija, R. Kotte, M. Kowalczyk, T. Kress, R. Kutsche, A. Lebedev, K. S. Lee, V. Manko, H. Merlitz, S. Mohren, D. Moisa, J. Mönsner, W. Neubert, A. Nianine, D. Pelte, M. Petrovici, C. Pinkenburg, C. Plettner, W. Reisdorf, J. Ritman, D. Schüll, Z. Seres, B. Sikora, K. S. Sim, V. Simion, K. Siwek-

- Wilczyńska, A. Somov, M. R. Stockmeier, G. Stoicea, M. Vasiliev, P. Wagner, K. Wiśniewski, D. Wohlfarth, J. T. Yang, I. Yushmanov, A. Zhilin, and F. Collaboration), Phys. Rev. Lett. **84**, 1120 (2000).
- [37] P. Danielewicz, R. Lacey, and W. G. Lynch, Science **298**, 1592 (2002).
- [38] C. Hartnack, R. K. Puri, J. Aichelin, J. Konopka, S. A. Bass, H. Stöcker, and W. Greiner, EPJ A **1**, 151 (1998).
- [39] J. Blaizot, J. Berger, J. Dechargé, and M. Girod, Nuclear Physics A **591**, 435 (1995).
- [40] P. Danielewicz, Physics Letters B **146**, 168 (1984).
- [41] L. Shi and P. Danielewicz, Phys. Rev. C **68**, 064604 (2003).
- [42] G. Bertsch and J. Cugnon, Phys. Rev. C **24**, 2514 (1981).
- [43] L. Csernai and J. I. Kapusta, Physics Reports **131**, 223 (1986).
- [44] G. F. Bertsch, Nuclear Physics A **400**, 221 (1983).
- [45] M. L. Miller, K. Reygers, S. J. Sanders, and P. Steinberg, Annu. Rev. Nucl. Part. Sci. **57**, 205 (2007).
- [46] A. Adil, H.-J. Drescher, A. Dumitru, A. Hayashigaki, and Y. Nara, Phys. Rev. C **74**, 044905 (2006).
- [47] J. E. Bernhard, P. W. Marcy, C. E. Coleman-Smith, S. Huzurbazar, R. L. Wolpert, and S. A. Bass, Phys. Rev. C **91**, 054910 (2015).
- [48] F. Karsch, E. Laermann, and A. Peikert, Nuclear Physics B **605**, 579 (2001).